Biaxial melting of the nematic order under a strong electric field

Ph. Martinot-Lagarde,[1,2] H. Dreyfus-Lambez,[1] and I. Dozov[2]
[1]*Laboratoire de Physique des Solides, Université Paris-Sud, bat. 510, F-91405 Orsay, France*
[2]*Nemoptic, Parc du Mérantais, 1 rue Guynemer, F-78114 Magny-les-Hameaux, France*
(Received 5 November 2002; published 28 May 2003)

We study the action of a strong electric field on a nematic, topologically stabilized with director **n** perpendicular to **E**. Above a threshold field the nematic order on the cell midplane is ''melted'' and rapidly reconstructed with $\mathbf{n}\|\mathbf{E}$. In a Landau–de Gennes model, we show that the observed transient ''melted'' state is a biaxial nematic and not an isotropic liquid.

DOI: 10.1103/PhysRevE.67.051710 PACS number(s): 61.30.Gd, 61.30.Cz, 64.70.Md

Nematic liquid crystals are fluids with orientational order described by a tensor order parameter **Q**. In the ground state, **Q** is uniform and uniaxial, $Q_{ij}=S(n_in_j-\delta_{ij}/3)$ where **n** is the director and S is the scalar order parameter. Nematics are easily oriented by electric fields, due to their weak elasticity and strong dielectric anisotropy $\Delta\varepsilon$ (we suppose $\Delta\varepsilon>0$, favoring $\mathbf{n}||\mathbf{E}$). The length scale of the director distortion, the electric correlation length ξ_E [1], is macroscopic for moderate fields ($\xi_E\sim 200$ nm for $\Delta\varepsilon=10\ \varepsilon_0$ and $E=1$ V/μm).

The field coupling with S induces an order variation $\delta S=S-S_0$. S being much ''stiffer'' [1] than **n**, S relaxes at the scale of the nematic coherence length ξ_N (a few nanometers). Strong fields enhance the bulk order [2] or induce $S\neq 0$ in the isotropic melt [3]. By symmetry, the induced order tensor **Q** is uniaxial like the spontaneous one.

When $\mathbf{E}\perp\mathbf{n}$, we expect field induced disorder and some biaxiality—the field breaks the symmetry of the phase. However, experimentally it is difficult to stabilize $\mathbf{n}\perp\mathbf{E}$—the dielectric torque favors $\mathbf{n}\|\mathbf{E}$. Even strong surface anchoring does not keep $\mathbf{n}\perp\mathbf{E}$—for high enough fields $\xi_E\approx\xi_N\ll L$ (L is the surface extrapolation length [1]) and the anchoring is broken [4]. So far, field induced disorder and biaxiality have been reported [5] only in the isotropic phase, perturbing the surface induced order.

The nematic order decreases and even vanishes under strong topological constraint, e.g. in the core of a 1/2 strength disclination line or in a point defect [1]. Due to the broken symmetry, the core is not isotropic ($S=0$) but becomes strongly biaxial [6]—**Q** varies continuously in the core, without vanishing, enabling an escape from the topological constraint imposed on the director.

Here, to study the nematic behavior under a strong electric field $\mathbf{E}\perp\mathbf{n}$, we use a thin cell with inverse pretilt. By symmetry, $\mathbf{n}\perp\mathbf{E}$ in the middle of the cell. Above a threshold field we observe transient ''melting'' of S all over the cell midplane, with escape from the topological constraint, followed by a fast reconstruction of the order with $\mathbf{n}\perp\mathbf{E}$. In a Landau–de Gennes model, we show that the transient melted state is a biaxial nematic and not an isotropic liquid.

Our experimental cells are 1.5 μm thick with inverse pretilt ψ (texture U in Fig. 1), ranging from 2° (brushed polymer) to 30° (SiO evaporation), filled with the nematic pentyl cyanobiphenyl (5CB Merck). The field $E\leqslant 30$ V/μm is applied along the cell normal in short ac bursts ($f\geqslant 100$ kHz to avoid polar effects) of square envelope, with duration $\tau=1\ \mu$s–10 ms. In the two boundary regions, **n** reorients along **E**, while in the center of the cell $\mathbf{n}\perp\mathbf{E}$ and the electric torque vanishes (texture W in Fig. 1). This results in a thin ($\sim 2\xi_E$) π wall of splay bend, blocked in the middle of the cell. At long term, the wall could migrate to one of the boundaries, breaking eventually the surface anchoring [4]. However, for $E>2$ V/μm the wall propagation is very slow (minutes), and on the time scale of our experiments the texture W is dynamically stabilized (in this geometry, the anchoring cannot break [4]).

Under field, a large excess energy is concentrated in the wall, compared to the texture H (Fig. 1) realized with the same anchorings. However, a continuous transition of W into H is impossible. Instead, the transition can be intermediated by defects—a π-disclination line, propagating along the wall, replaces locally W by H, the melted order in the line core enabling the topological constraint escape.

Let us first suppose that there is no defect propagation. On increasing the field, S in the wall should decrease, due to the field action and the strong distortion. At high enough field, we expect a transient melting of S all over the wall plane, followed by rapid reconstruction of the nematic order, with $\mathbf{n}\|\mathbf{E}$ to give the texture H. In this way, the transient ''defect'' plane enables a fast uniform escape from the topological constraint [7], instead of a local transition by defect lines.

To detect this W to H transition, we observe the texture after the pulse. On field removal, W relaxes back to the highly birefringent texture U, while the texture H relaxes to a half-turn twisted texture T (Fig. 1), optically almost isotropic in thin cells [8]. Qualitatively, we observe two different behaviors, presented in Fig. 2, as a function of E and τ. Up to a critical field $E_c=7.8$ V/μm, we observe W to H transition

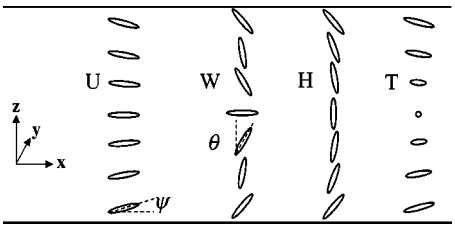

FIG. 1. Textures realized in the inverse pretilt cell without field (U,T) and under field (W,H).

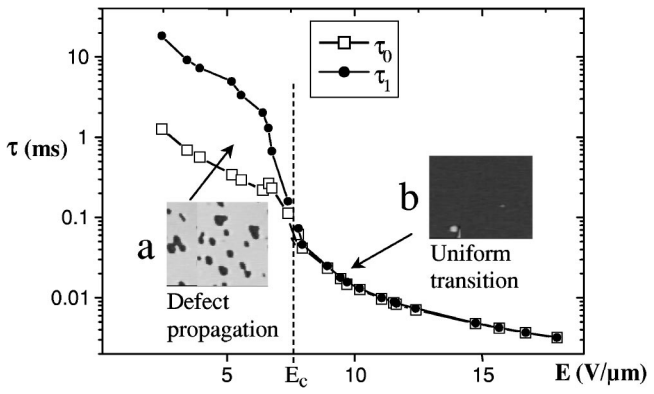

FIG. 2. Indirect observation of the W to H transition under field at $T_c - T = 5$ K; (a) defect propagation for $E < E_c$, (b) uniform melting of the wall for $E > E_c$.

by defect propagation, localized in small circular domains [photograph (a) in Fig. 2]. The twisted regions first appear at $\tau = \tau_0$ and grow with increasing τ, confirming defect propagation. For $\tau \geqslant \tau_1$, all the pixel transits to the texture H (and then T) by defect propagation.

Above E_c, $\tau = \tau_1$ and there is no more coexistence of U and T after the pulse. For $\tau < \tau_0$ whole pixel (several mm^2) relaxes back to U, for $\tau > \tau_0$ it changes to T [photograph (b) in Fig. 2], indicating a uniform melting of the wall under field. This behavior disagrees with defect propagation, implying a strong stepwise increase of the defect velocity (up to 10 m/s).

The W to H transition can also be detected in real time from the cell birefringence. Optically, W differs from H by the additional birefringence of the wall ($\delta \sim \Delta n \xi_E \sim 1$ nm). We measure it with an experimental setup [9] mounted on a polarizing microscope, with a good resolution in time (1 μs) and in δ (0.01 nm).

For $E < E_c$ (Fig. 3, curve *a*) δ saturates to a first level, corresponding to the texture W, and then slowly ($\Delta \tau_a \sim 10$ ms) relaxes to a lower value (texture H, the wall has disappeared). $\Delta \tau_a$ increases with the observation area, indicating a transition by defect propagation. For E slightly above E_c (Fig. 3, curve *b*), the wall disappears much faster ($\Delta \tau_b \sim 100$ μs). $\Delta \tau_b$ is independent of the observed area, indicating a synchronous transition over the whole pixel (either by uniform melting or by spinodal decomposition). After the pulse, the texture relaxes uniformly to U or to T, for pulse duration, respectively, in the first or in the second plateau in Fig. 3. Finally, for $E \gg E_c$, the wall melting cannot be

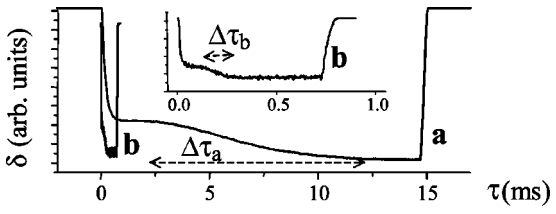

FIG. 3. Direct observation of the W to H transition from the cell birefringence; (a) defect propagation for $E < E_c$, (b) uniform transition at $E = 1.03 E_c$.

observed directly—the transition happens during the bulk relaxation and it is masked by the residual bulk birefringence.

Our experimental results can be understood in the frames of the Landau–de Gennes approach, minimizing the free energy $F(\mathbf{Q}, \nabla \mathbf{Q})$ [1]. In our geometry, the surfaces align **n** in the **x-z** plane. The electric field $\mathbf{E} \| \mathbf{z}$ induces some biaxiality but keeps **xz** as a mirror plane for the texture. With this symmetry, the most general form of the biaxial traceless tensor **Q** is

$$Q = \frac{1}{3} \begin{pmatrix} -\alpha - \sqrt{3}\beta \cos 2\theta & 0 & \sqrt{3}\beta \sin 2\theta \\ 0 & 2\alpha & 0 \\ \sqrt{3}\beta \sin 2\theta & 0 & -\alpha + \sqrt{3}\beta \cos 2\theta \end{pmatrix}. \tag{1}$$

Here θ (Fig. 1) describes the rotation of **Q** around **y** (one of its main axes), while α and β define together the modulus $S = \sqrt{\alpha^2 + b^2}$ and the biaxiality [proportional to $\beta(3\alpha^2 - \beta^2)/S^3$] of the order parameter.

The condensation energy density becomes

$$F_c = \frac{a(T - T^*)}{2}(\alpha^2 + \beta^2) + \frac{B}{3}\alpha(\alpha^2 - 3\beta^2) + \frac{C}{4}(\alpha^2 + \beta^2)^2, \tag{2}$$

where the numerical values for 5CB are [10] $a \approx 0.13$ J/(cm^3 K), $B \approx -1.6$ J/cm^3, and $C \approx 3.9$ J/cm^3.

The distortion energy density in one-constant approximation is [11]

$$F_d = \frac{L}{2}\partial_i Q_{jk} \partial_i Q_{jk} = \frac{L}{3}\left[\left(\frac{\partial \alpha}{\partial z}\right)^2 + \left(\frac{\partial \beta}{\partial z}\right)^2 + 4\beta^2\left(\frac{\partial \theta}{\partial z}\right)^2\right] \tag{3}$$

with $L = K/2S^2 \approx 8$ pN.

The electric energy density is

$$F_e = \frac{1}{2} D_z E_z = \frac{D_z^2}{2}\left[\varepsilon_{\perp 0} + \frac{\varepsilon_{a0}}{3}(1 - \alpha + \sqrt{3}\beta \cos 2\theta)\right]^{-1}, \tag{4}$$

where **D** is the electric displacement and $\varepsilon_{\perp 0} \approx 3 \times 10^{-11}$ F/m and $\varepsilon_{a0} \approx 18 \times 10^{-11}$ F/m are the permittivities of 5CB at $S = 1$ [12].

Let us first consider the condensation energy of a uniform nematic with fixed orientation $\theta \equiv 0$ and $\mathbf{E} = 0$, presented in Fig. 4. The three minima x, y, and z correspond to the uniaxial equilibrium states of the nematic, with $S = S_0(T)$, $\theta = 0$ and with **n**, respectively along x ($\alpha = -S/2$, $\beta = -\sqrt{3}S/2$), $\mathbf{y}(\alpha = S,\ \beta = 0)$, or $\mathbf{z}(\alpha = -S/2,\ \beta = \sqrt{3}S/2)$. The maximum **I** at $\alpha = \beta = 0$ represents the isotropic state ($S = 0$). Along X, Y, and Z the **Q** tensor is uniaxial, either prolate ($S > 0$ on the X,Y,Z positive side) or oblate ($S < 0$ on the X,Y,Z negative side). The three saddle points x', y', and z' represent the known unstable uniaxial solutions with $S \approx -S_0/2$. All the other regions in the diagram represent biaxial nematic states, never realized without constraint. We note that the same results are obtained by fixing θ at $\theta = \pi/2$ and changing the sign of β.

In Fig. 5, we show the energy of the uniform nematic with $\theta \equiv 0$ under strong field $\mathbf{E} \| \mathbf{z}$. The state z (with $\mathbf{n} \| \mathbf{z}$) remains

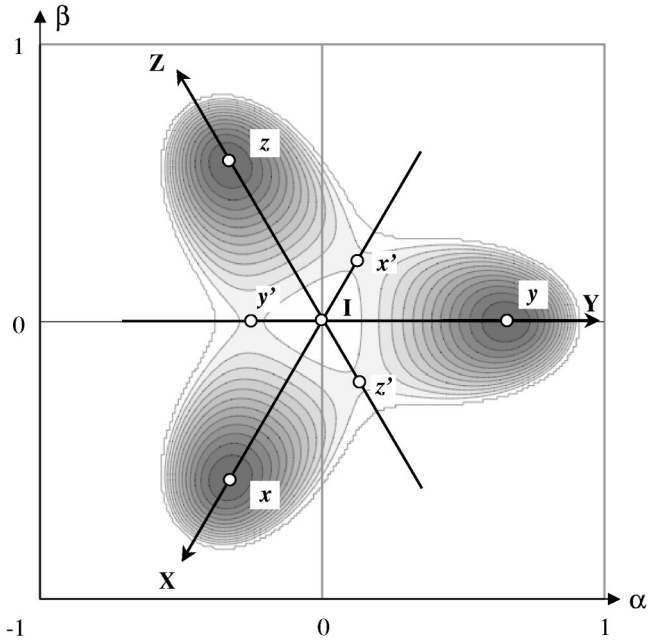

FIG. 4. Condensation energy map for a uniform nematic with fixed orientation $\theta \equiv 0$ (darker gray corresponds to lower energy).

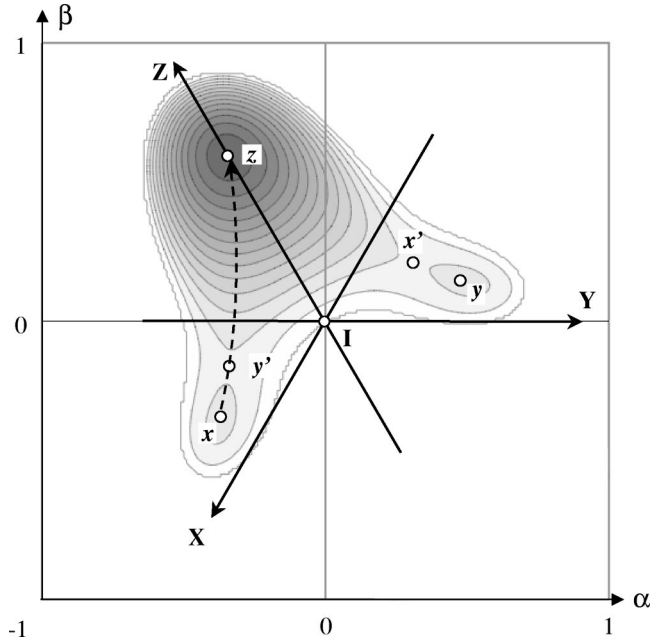

FIG. 5. Total energy map for a uniform nematic under strong field.

uniaxial, with order parameter $S > S_0$ enhanced by the field. In the metastable states x and y, the order decreases and becomes biaxial. When **E** is increased, x and y reach, respectively, the saddle points y' and x', and disappear at a critical field E_{cu}. From the condition of double extrema for $F_c + F_e$, we find algebraically [13]

$$E_{cu} = \sqrt{\frac{3B}{4\varepsilon_{a0}}\left(\frac{4a(T-T^*)}{C} - \frac{B^2}{C^2}\right)} \approx 67 \ \text{V}/\mu\text{m}$$

at $T_c - T = 5$ K.

When $E > E_{cu}$, one expects a field driven transition from the x or y state to the stable z state. Due to the "frozen" orientation ($\theta \equiv 0$), this transition is realized by variation of the **Q** eigenvalues. The **Q** trajectory (Fig. 5) explores a continuum of biaxial states and passes through a uniaxial oblate state [14].

In our experiments, we expect the same kind of transition from x to z in the wall midplane, where the topological constraint forbids the rotation of **Q**. Two phenomena help the transition and decrease the critical field for the wall melting: the nonuniformity of the field and the distortion in the wall. Under field most of the sample is homeotropic, with $D_z \approx \varepsilon_\parallel U/d$. In the middle of the wall, the field is $E_z = D_z/\varepsilon_{zz} \approx (\varepsilon_\parallel/\varepsilon_\perp)U/d$; three times stronger for 5CB at room temperature than the average field $E = U/d$.

The distortion in the wall decreases the nematic order, and to estimate this effect we need to consider the space variation of α, β, and θ. We solve numerically the Euler-Lagrange equations at fixed D_z values using a relaxation algorithm and we obtain U by integrating D_z/ε_{zz}. We impose strong boundary conditions $\alpha_S = -S_0/2$, $\beta_S = \sqrt{3}S_0/2$, and $\theta_S = \pi/2 \pm \psi$. These conditions influence only the two thin ($\sim \xi_E$) regions close to the surfaces, where α and β relax to their bulk equilibrium values under field and θ goes to $\theta \approx 0$. In Fig. 6, we present in the ($\beta \cos 2\theta$, $\beta \sin 2\theta$) space the numerically calculated path $\mathbf{Q}(z)$. For simplicity, we do not present the surface regions part of the path nor $\alpha(z)$ ($\alpha \approx -S_0/2$ and approximately constant). The circle $\beta = \beta_0 = S_0\sqrt{3}/2$ represents the equilibrium uniaxial prolate state with $S = S_0$ and simple director rotation. The center of the diagram D corresponds to the uniaxial oblate state with $S < 0$. All the other states inside the circle β_0 are biaxial (prolate close to β_0, oblate close to D). Far from the wall, the nematic is in the state z ($\theta = 0$ or π).

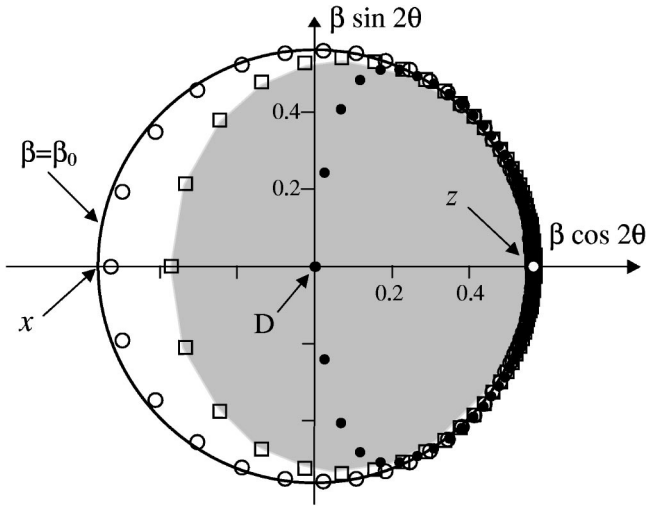

FIG. 6. Numerical results for the equilibrium and transient $\mathbf{Q}(z)$ trajectories across the wall as a function of the field. The equilibrium states are forbidden in the shaded region: $E = 0$ (line); $E = E_{cd}/2$ (open circles); $E = E_{cd}$ (squares); and $E = 1.03E_{cd}$ (closed circles).

For weak fields (Fig. 6, open circles) **Q** explores a loop close to β_0, starting from the state $z(\mathbf{n}\|\mathbf{z})$, crossing the state $x(\mathbf{n}\|\mathbf{x})$, and finishing again at z, but now with $\mathbf{n}\|-\mathbf{z}$, accumulating a ''phase shift'' $\Delta\theta=\pi$ across the wall. Each point on the curve corresponds to a step 0.1 ξ_E along z, to visualize $\nabla\mathbf{Q}$. For higher fields, up to a threshold $E_{cd}=15.2$ V/μm (Fig. 6, squares), the path goes deeper in the biaxial region, especially for $\theta=\pi/2$. Finally, above E_{cd}, the Euler-Lagrange equations have no solution for the imposed boundary conditions. In the present static model, this corresponds to a first-order jump of the texture W toward the homeotropic state H (the point z, with $\mathbf{n}\|\mathbf{z}$ and $S>S_0$ due to the field-induced order). A dynamical model, to be presented elsewhere, confirms the first-order transition, with the loop collapsing rapidly toward the point z. The intermediate nonequilibrium trajectories (e.g., Fig. 6, closed circles) explore all the biaxial states of the diagram. When the loop crosses the oblate uniaxial state D, the phase shift across the wall jumps from $\Delta\theta=\pi$ to $\Delta\theta=0$, removing the initially imposed topological constraint.

The experimentally observed threshold E_c should be compared with the threshold E_{cd}, calculated for the biaxial melting of the distorted wall, four times lower than the value E_{cu} calculated for uniform nematic. The large decrease of E_{cd} (compared to E_{cu}) results from the strong electric torque applied on the nematic in the regions with $|\theta|\approx\pi/4$, and elastically transmitted to the middle of the wall, where the nematic order is already destabilized by the strong distortion and the direct action of the electric field. However, at $T_c-T=5$ K, E_{cd} is still two times higher than E_c. This disagreement can be attributed to the known limitations of the Landau–de Gennes approach, namely, the bad convergence of the Eq. (2) series, needing higher-order terms [2]. Moreover, E_c/E_{cd} varies with the temperature (to be presented in a forthcoming paper), confirming the quantitative disagreement between the present model and the experiment. We observe qualitatively the same trends and similar values of E_c and E_{cd} for several other nematics with high $\Delta\varepsilon/\epsilon_\perp$ anisotropy, with biaxial melting of the wall observed for $E_c<30$ V/μm even at low temperatures ($T_c-T=25$ K).

The shaded region in Fig. 6 corresponds to a transient state of the wall, melted into an unstable highly biaxial state. The melted wall can be considered as a ''core'' of a transient nematic two-dimensional (2D) ''defect,'' nematic analog to the permanent 2D defects already reported for the smectic phase [15]. This 2D core enables biaxial escape (in the *time*) from the imposed topological constraint, similar to what happens (in the *space*) around the 1D core of 1/2 strength disclination line.

To conclude, we realize and observe experimentally a biaxial melting transition in nematic liquid crystals under strong topological constraint and destabilizing electric field $\mathbf{E}\perp\mathbf{n}$. A qualitative agreement with the experiment is obtained in a Landau–de Gennes model. Even far away from the clearing temperature, this rapid transition (micro second time scale) has moderate field threshold (<30 V/μm), showing potential for rapid nematic applications [16].

[1] P.G. de Gennes and J. Prost, *The Physics of Liquid Crystals* (Clarendon Press, Oxford, 1993).

[2] I. Lelidis, M. Nobili, and G. Durand, Phys. Rev. E **48**, 3818 (1993).

[3] I. Lelidis and G. Durand, Phys. Rev. E **48**, 3822 (1993).

[4] I. Dozov and Ph. Martinot-Lagarde, Phys. Rev. E **58**, 7442 (1998).

[5] J.H. Kim, R.G. Petschek, and C. Rosenblatt, Phys. Rev. E **60**, 5600 (1999).

[6] N. Schopohl and T.J. Sluckin, Phys. Rev. Lett. **59**, 2582 (1987).

[7] Ph. Martinot-Lagarde, H. Dreyfus-Lambez, and I. Dozov (unpublished).

[8] I. Dozov *et al.*, Proc. SPIE **3015**, 61 (1997).

[9] S. Lamarque-Forget, P. Martinot-Lagarde, and I. Dozov, Jpn. J. Appl. Phys., Part 2 **40**, L349 (2001).

[10] H.J. Coles, Mol. Cryst. Liq. Cryst. Lett. **49**, 67 (1978).

[11] E.B. Priestley, P.J. Wojtowitcz, and P. Sheng, *Introduction to Liquid Crystals* (Plenum Press, New York, 1976).

[12] B.R. Ratna and R. Shashidhar, Mol. Cryst. Liq. Cryst. **42**, 113 (1977).

[13] Technically it is easier to obtain this analytical result by ''applying'' the field along the y axis. Then, the axis Y in Fig. 5 remains a symmetry element of the system under field and the algebra is greatly simplified.

[14] Except above the temperature $T^*\sim T_c-1$ K, where the nematic and isotropic phases can coexist. In this pretransitional case, the saddle points x',y' and z' disappear, and the transition trajectory passes through the isotropic state.

[15] I. Dozov and G. Durand, Europhys. Lett. **28**, 25 (1994); I. Dozov, Phys. Rev. Lett. **74**, 4245 (1995).

[16] Ph. Martinot-Lagarde and I. Dozov, French Patent No. FR280889 (16.11.2001).